A. D. K. LAIRD and DUNCAN CHISHOLM
University of California, Berkeley, Calif.

Pressure and Forces along Cylindrical Bubbles in a Vertical Tube

BECAUSE large bubbles appear to be the dominant feature of cocurrent gas-liquid flow in vertical tubes at low rates, their behavior is important to an understanding of the general phenomenon of gas-liquid flow.

Davies and Taylor (*1*) gave a good approximation for the shape of a large bubble in a vertical open end tube, but indicated that more work was needed to account for viscous effects near the tube wall.

In the present research the bubbles were admitted singly into the bottom of a column of water standing in a vertical tube of Lucite acrylic resin, 38 feet long and 2 inches in inside diameter. The experimental work was principally intended to measure the variation of pressure along the bubble. The velocity of the bubbles as a function of length and the shear force exerted by the water upon the tube walls were also measured.

Equipment

The pressures were measured by Wiancko reluctance-type pressure pickups and recorded by a Brush Electronic Co. magnetic oscillograph with a sensitivity of 0.1 inch of water and a time response of 40 cycles per second (*2*).

The three arrangements for measuring the bubble behavior are shown in Figure 1,*a*, *b*, and *c*. As shown in Figure 1,*a*, the oscillograph was attached to the upper and lower taps set 9 inches apart on the 2-inch Lucite tube. The 16-mm. camera viewed the flow tube, stop watch, linear scale, and oscillograph with the aid of the mirror.

To reduce refraction in viewing the bubbles, a square-sectioned Lucite viewing box 16 inches long was constructed around the tube; water filled the space between the tube and box. The pressure pickups were calibrated by loading them with water in the 2-inch tube to known heights above their respective pressure taps. Their cases were open to the atmosphere. After calibration, the tube water level was raised and air, compressed by a mercury column, was admitted to the cases to counterbalance the static water pressure and thereby center up the oscillographs. A suitable volume of air was then admitted at the bottom of the tube. By the time most of the air coalesced into a bubble and the pendulation of the water column had decreased appreciably, the bubble had risen to the bottom of the view box and the camera was started.

Four kinds of lighting were used. Right-side lighting by a beam between $1/8$ and $3/16$ inch in breadth and 10 inches long, directed along the diameter perpendicular to the camera's line of sight, was used first. Then one photo floodlight was added to illuminate the tube from the left and above. Next, a second floodlight was added from the right and below. Finally, only backlighting by another floodlight was employed. The second and last lightings gave the best detail.

The second arrangement, shown in Figure 1,*b*, was used as a further check on the pressure variation as the bubble passed the pressure taps. One Wiancko pressure element was connected differentially between the pressure taps, indicating the difference in pressure along the bubble. The bubble length was estimated visually as it passed the pressure taps.

The arrangement in Figure 1,*c*, used the same bubble tube as in 1,*a*. The oscillographs were replaced by one water manometer parallel to the 2-inch tube and connected to the upper of the two pressure taps at the view box. The water in the saran tube $1/4$ inch in outside diameter was tinted with potassium permanganate. Two men recorded the various levels of the water in the 2-inch and $1/4$-inch tubes as the bubbles ascended. A third observer timed the rise of the bubble between two levels. A fourth estimated the bubble length as it passed the manometer connection. The camera was set at the level of the water surface and two mirrors brought the view box into the field of the camera.

Results

Figure 2 presents the variation of bubble velocity between 0.78 and 0.88 foot per second for lengths between 2 and 47 inches, respectively.

Figure 3 shows the changes in manometer level (Figure 1,*c*) due to the disappearance of the wall shear forces as the bubbles broke the surface.

Figure 4 gives the wall pressure-time and bubble position-time history for a

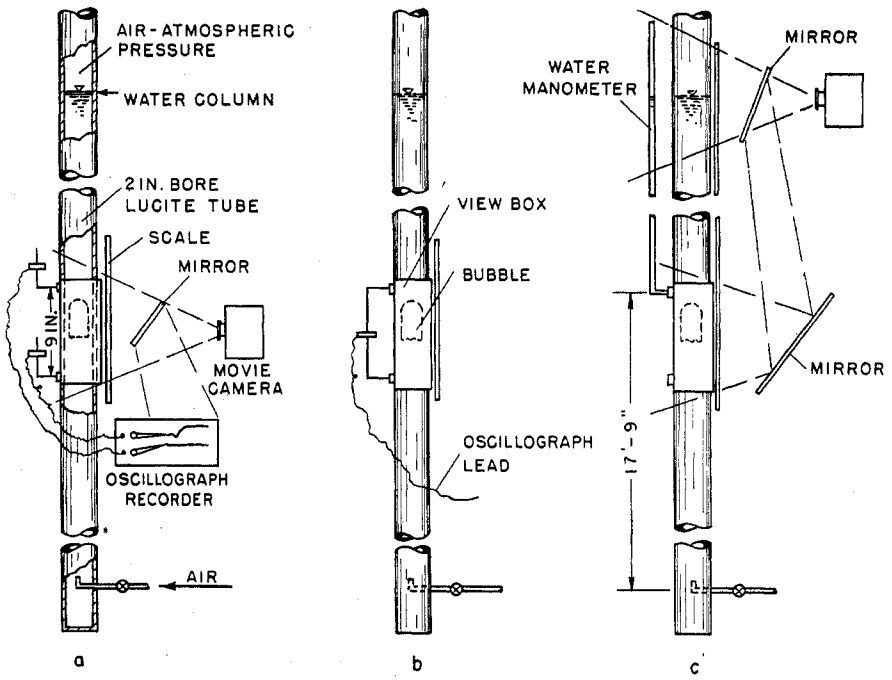

Figure 1. Experimental equipment

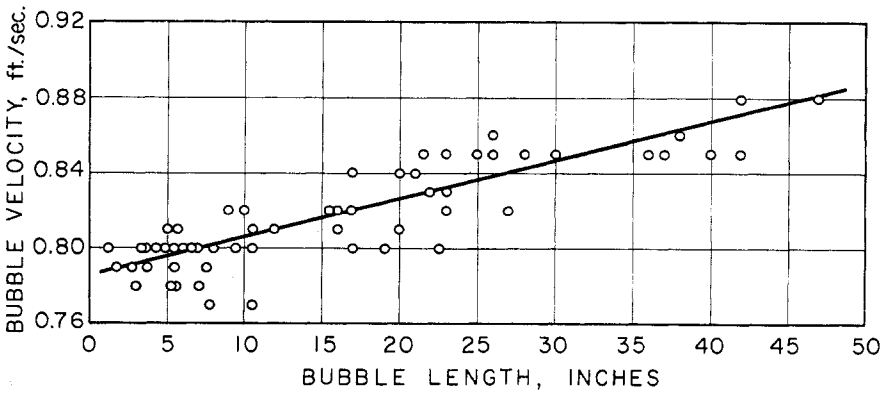

Figure 2. Bubble velocity *vs.* bubble length

bubble as it ascended past the pressure taps.

Figure 5 shows the difference between the pressures at the upper and lower pressure taps as measured from separate oscillograph traces, and the measured differential pressure between the same taps for two bubbles approximately 7.6 inches long.

Figure 6 gives representative differential pressure traces over the range of bubble lengths.

Discussion

The rate of rise of bubbles (Figure 2) shows the scatter that might be expected under experimental conditions. The velocities and bubble lengths measured on the film gave confirmation of values obtained visually. The bubble lengths estimated visually have occasional deviations of as much as 10%. The exposure time caused the bubble nose to appear about 1/8 inch thick, but this thickening had little effect on the accuracy of the velocity measurements. The stop-watch timing over a distance of 6 feet might result in occasional errors of 3%.

Taylor's equation

$$U_t = 0.464\sqrt{ga} \qquad (1)$$

gives a bubble velocity, U_b, of 0.76 foot per second for a tube of radius a, equal to 1 inch. The corresponding observed velocity range was from 0.78 to 0.88 foot per second.

The pictures and oscillograph traces showed a time lag of about 0.1 second between the time the bubble nose reached a pressure tap and that at which the pressure changed. In this time, the nose of the bubble had risen a distance of approximately one tube radius above the pressure tap. As the velocity head of the water along the bubble surface is equal to the vertical distance below the bubble vertex, some viscosity and momentum effects may keep the pressure up during this first 0.1 second.

The shapes of the bubbles were not measured, because of the lack of definition in the films. The lighting produced apparent bubble sides which were asymmetric. Consequently, it was assumed that the light reflections were not from the exact sides of the bubbles and the resulting shapes were misleading. The approximate shapes, however, checked well with those reported by Davies and Taylor (*7*).

The liquid extending from well above to well below the bubble may be considered as an ordinary free body. The difference in the pressure forces on the top and bottom must be balanced by the buoyant force of the bubble and the shear force on the tube wall. The downward direction of the water past the bubble necessitates the existence of a shear force which helps to support the water column. As the bubble breaks through the upper surface of the water column, the shear force vanishes and the pressure below the bubble increases by an amount equal to the shear force divided by the cross-sectional area of the tube. This pressure change, p_s, was measured by observing the increase in manometer level, h, as the bubble broke the surface (Figure 1,*c*). The resulting data lie about the curve

$$h = 0.0128L^{1.5} \qquad (2)$$

where L is the bubble length. The pressure change is related to the shear stress, τ, on the tube wall, and to the change in manometer level, in the equations

$$p_s = \tau A_s/A \qquad (3)$$

$$p_s = h\rho_L \qquad (4)$$

where A is the tube cross section, A_s is the surface area of the tube wall on which the shear force acts, and ρ_L is the water density.

Because a rigorous solution for the distribution of a viscous fluid along a bubble is not available, an approximate solution, using the "free fall" assumption given by Davies and Taylor (*7*), will be developed.

The downward water velocity at a point x below the bubble vertex is

$$U = \sqrt{2gx} \qquad (5)$$

The shear forces at the wall are neglected. At all sections the flow volume upward equals the flow volume downward (no change in the water surface level). Hence,

$$UA_w = U_b(A - A_w) \qquad (6)$$

where A_w is the cross section occupied by

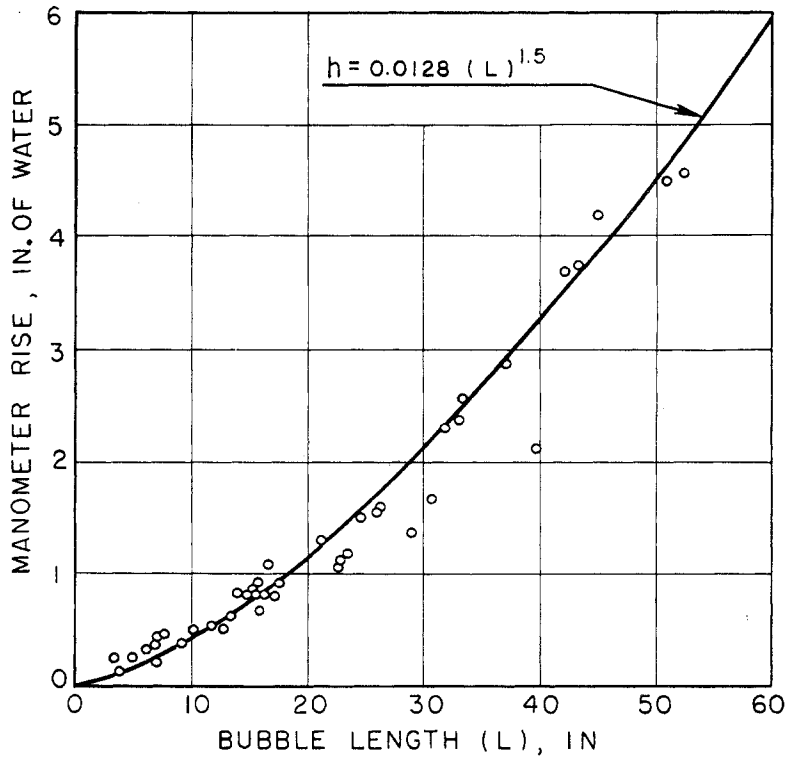

Figure 3. Apparent pipe wall shear force *vs.* bubble length

water, A is the cross section of the tube, and U_b is the upward velocity of the bubble (mean value of 0.83 used). The volume of water along length dx of the bubble, as found by combining equations, is

$$A_w dx = \frac{A dx}{1 + \frac{\sqrt{2gx}}{U_b}} \qquad (7)$$

The rise, δL, of the water surface after the collapse of the bubble is the volume of the water along the bubble divided by the tube cross section.

$$\delta L = \int_0^L \left(1 + \frac{\sqrt{2gx}}{U_b}\right)^{-1} dx \qquad (8)$$

$$\delta L = \frac{U_b^2}{g}\left[\frac{\sqrt{2gL}}{U_b} - \ln\left(1 + \frac{\sqrt{2gL}}{U_b}\right)\right] \qquad (9)$$

In the absence of small bubbles in the wake of the main bubble, the increase in surface level due to the bubble collapse indicates the volume of water along the sides of the main bubble. Most of the small bubbles following the main bubble were so far behind that the rise of the water surface after collapse of the main bubble could be measured before much of the following air reached the free surface. The photographic records provided a total of six determinations of surface rise. These observed values and the theoretical curve of Equation 9 plotted in Figure 7 are in good agreement. The assumption of free fall will give theoretical values that are too low; air in the wake close behind the bubble will cause the measured values to be too low. These two effects appear to be of the same magnitude in the region covered by the present investigation. Although this agreement between the calculated and measured values suggests that water is distributed along the bubble as indicated by Equation 7, it should not be assumed that Equation 7 will apply to a more viscous liquid.

Inspection of the pressure-time curves in Figures 4 to 7 shows that the pressure drop over the bubble length is practically zero, and it is considered zero in developing the following pressure relationships. With reference to Figure 9, if p_1 is the pressure at the bubble nose, then p_1 is also the pressure at the bubble tail, and consequently the pressure at point 3 is

$$p_3 = p_1 + x\rho_L + KE_R \qquad (10)$$

where KE_R is the kinetic energy recovery and x is the distance of point 3 below the bubble nose.

If p_3 is in a region where there is no liquid motion, the pressure may also be stated as

$$p_3 = (x - L)\rho_L + p_1 + \delta L\rho_L - p_s \qquad (11)$$

where $\delta L\rho_L$ is the pressure change due to the weight of water along the bubble

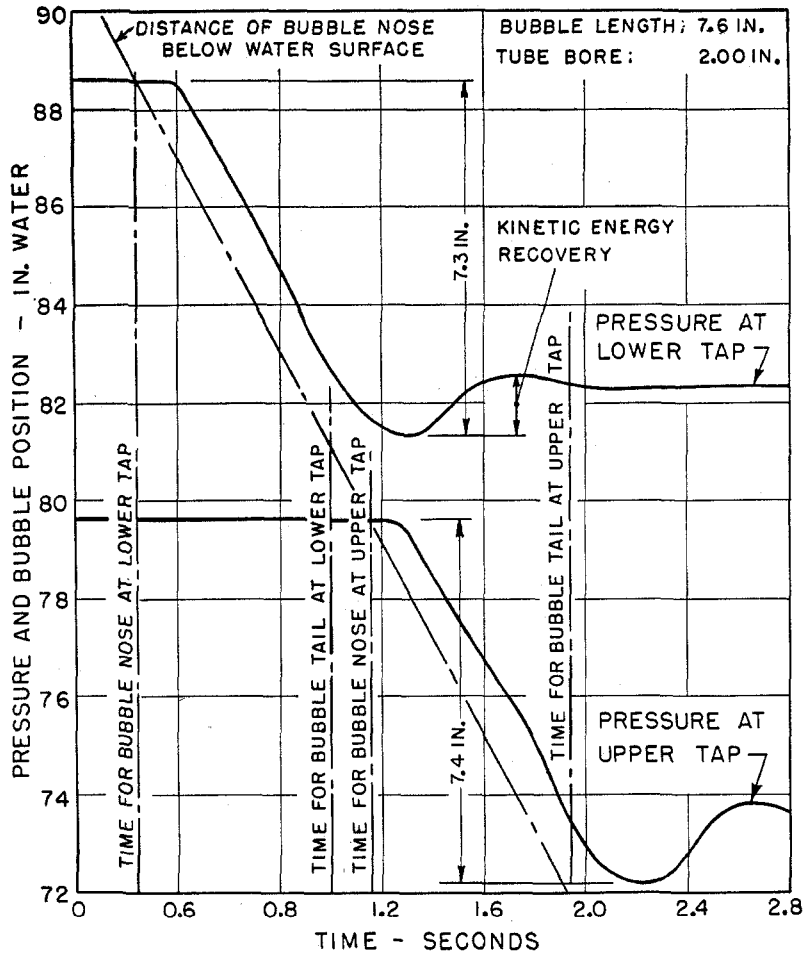

Figure 4. Tap pressure and bubble position vs. time. Bubble length 7.6 inches

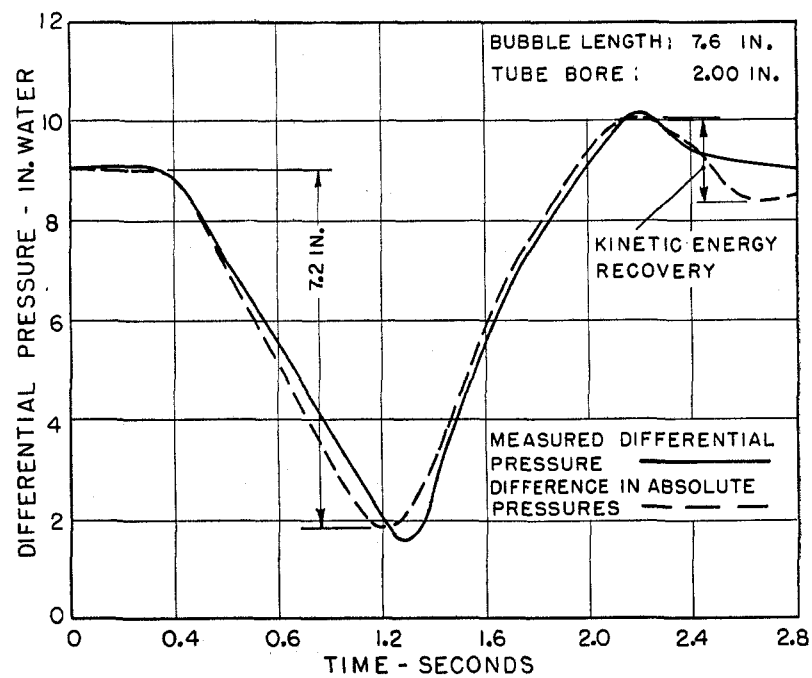

Figure 5. Differential pressure vs. time. Bubble length 7.6 inches

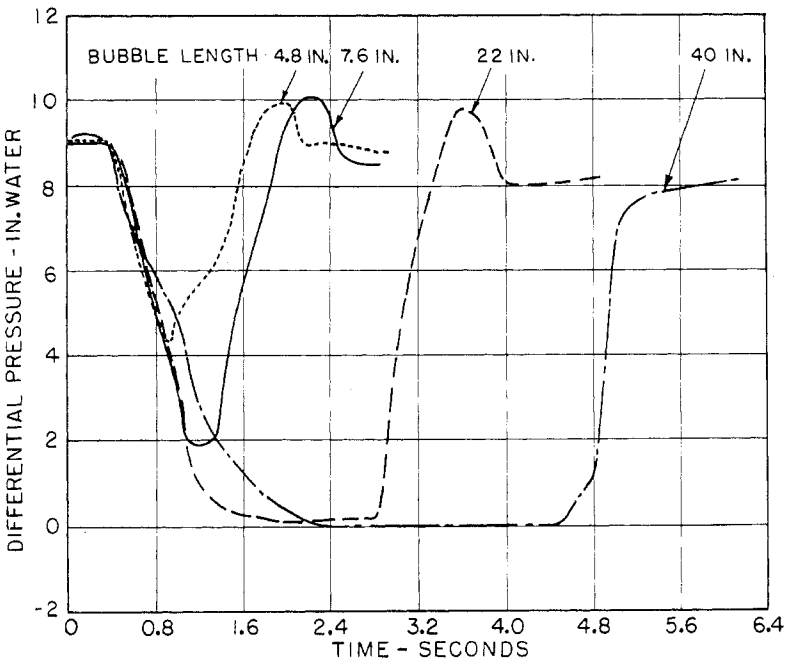

Figure 6. Differential pressure *vs.* time. Examples at different lengths

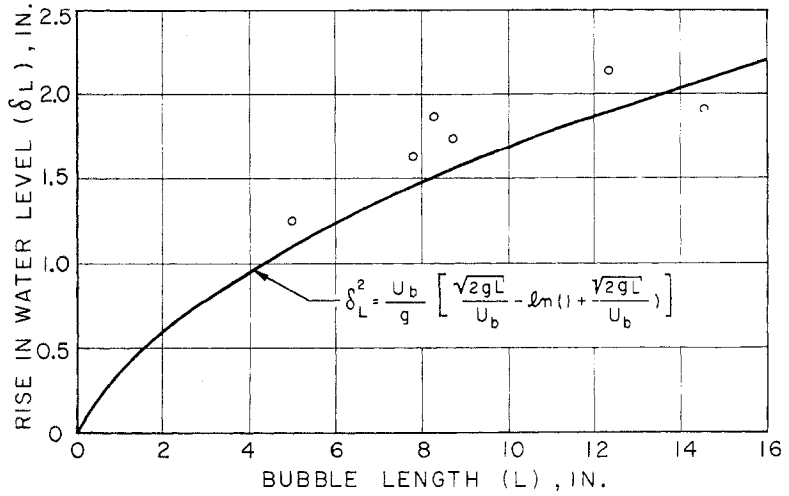

Figure 7. Comparison of measured rise of water level due to bubble collapse at surface and theoretical value predicted from liquid distribution around bubble

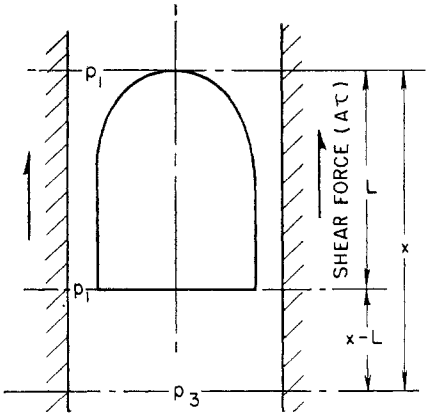

Figure 8. Diagrammatic sketch of bubble pressures and forces

wall and p_s is the pressure change due to the wall shear force.

Equating 10 and 11 gives

$$KE_R = \delta L \rho_L - p_s \qquad (12)$$

An approximate measurement of the kinetic energy pressure recovery was obtained from the pressure-time curves of Figures 4 and 5. Because air bubbles were present in the main bubble wake, the values are approximate only. Table I compares the kinetic energy recovery as obtained from the pressure-time curves and as estimated from Equation 12. Where pressure records were available for both upstream and downstream tap, both values are given. For the longer bubbles, no observed recovery of pressure was seen, and a trend in this direction in the estimated values may also be observed.

Conclusions

This investigation has studied forces and pressures acting on large bubbles rising in a vertical tube. The salient characteristics of these force and pressure actions are as follows:

Pressure drop is zero over most of the bubble length.

The shear force at the wall acts upward on the water column, and is proportional to the bubble length to the 1.5th power.

The measured kinetic energy recovery gives good agreement with values estimated from the other forces except with the larger bubbles.

Further study of this phenomenon is required.

The assumption that there is free fall of the liquid along the bubble wall gives good agreement with observations. The measured velocities of the bubble were on the average 10% greater than those obtained from the equations of Davies and Taylor.

Table I. Kinetic Energy Recovery

Bubble Length, Inches	Kinetic Energy Recovery, Inches of Water	
	Theoretical	Measured
4.8	0.92	1.2/1.6
7.6	1.19	1.6/1.3
22	1.3	1.8
40	0.3	...

Nomenclature

- A = tube cross-sectional area
- A_s = tube surface area on which shear forces act
- A_w = tube cross section occupied by water
- a = tube radius
- g = gravitational constant
- h = rise in manometer level
- KE_R = recovery of pressure due to kinetic energy changes at bubble tail
- L = bubble length
- δL = volume of water along bubble divided by tube cross section
- p = pressure
- p_s = pressure change due to wall shear forces
- U = water velocity
- U_b = bubble velocity
- x = distance below bubble vertex
- ρ_L = water density
- τ = wall shear stress

Literature Cited

(1) Davies, R. M., Taylor, Sir Geoffrey, *Proc. Roy. Soc.* (*London*) **200A,** 1062 (1950).

(2) Laird, A. D. K., *Trans. Am. Geophys. Union* **36,** No. 2, 279 (1955).

Received for review September 26, 1955
Accepted January 24, 1956
American Institute of Chemical Engineers, Detroit, Mich., 1955.